energy&fuels

Article

pubs.acs.org/EF

Pyrolysis of a Naturally Dried *Botryococcus braunii* Residue

Leonito O. Garciano II,[†] Nguyen H. Tran,[†] G. S. Kamali Kannangara,*[,†] Adriyan S. Milev,[†] Michael A. Wilson,[†,‡] David M. McKirdy,[§] and P. Anthony Hall[§]

[†]School of Science and Health, University of Western Sydney, Locked Bag 1797, Penrith, New South Wales 2751, Australia

[‡]Commonwealth Scientific and Industrial Research Organisation (CSIRO) Earth Sciences and Resource Engineering, Riverside Corporate Park, 11 Julius Avenue, North Ryde, New South Wales 2113, Australia

[§]Centre for Tectonics, Resources and Exploration (TRaX), School of Earth and Environmental Sciences, Mawson Laboratories, DP 313, University of Adelaide, Adelaide, South Australia 5005, Australia

ABSTRACT: The extant chlorophyte microalga *Botryococcus braunii* is a potential source of biofuel. In any future biofuel plant, it may be dried and stockpiled after harvesting and then pyrolyzed to generate oil. To investigate the formation of bio-oil from *B. braunii*, its naturally occurring residue known as coorongite was pyrolyzed non-isothermally and isothermally under about 1 atm of pure nitrogen carrier gas. The apparent pyrolysis activation energy of coorongite (25 kJ/mol) is much lower than those of most kerogens, which are on the order of 130−250 kJ/mol. However, it approaches that reported for a Moroccan marine oil shale, implying similarities in their responses to pyrolysis. Non-isothermal pyrolysis by thermogravimetry coupled with infrared spectroscopy (TG−IR) revealed coorongite to contain a significant amount of alkanes. Molecular analysis of the isothermal pyrolysates by gas chromatography−mass spectrometry (GC−MS) identified a homologous series of normal alkanes and alkenes (C_9−C_{21}), normal ketones (C_8−C_{12}), alkylaromatic compounds, carboxylic acids, and phenols. Structural group quantitation by nuclear magnetic resonance (NMR) and infrared (IR) spectroscopy showed that the pyrolysate is the result of several processes, with thermal decarboxylation forming alkanes, dehydrogenation ± cyclization forming alkenes and aromatic hydrocarbons, and some compounds being products of simple physical volatilization. Complementary analysis of the pyrolysis residues using solid-state ^{13}C NMR and IR revealed that their sp^3C−H carbon atoms would also be volatilized if treated by hydrocracking. These results suggest that stockpiled *B. braunii* may benefit from pyrolytic removal of carboxyl groups prior to further upgrading by hydrocracking and hydrogenation.

1. INTRODUCTION

With growing awareness of the adverse impacts of fossil fuel combustion on the global environment, interest is being rekindled in renewable biofuels from agricultural crops and microalgae. A wide range of processes have been developed for the recovery of fuels from such feedstock, some involving direct extraction and others involving fast, flash, or conventional pyrolysis.[1] They can generally be grouped into one of four categories according to which biopolymer or class of compounds is the principal fuel precursor. Oils produced from lignin are highly phenolic, making them suitable only as bunker fuel. Those derived from carbohydrates may be difficult to process because of their furan content. Arguably, the most successful are those derived from land or marine plants rich in glycerides. However, even these are not without problems (e.g., the need to remove oxygen and a lack of stability). Finally, there are algae that synthesize terpenes, although these have yet to be investigated in as much detail.

One such species, the lacustrine chlorophyte *Botryococcus braunii*, is well-known as a potential source of non-oxygenated, liquid fuels.[2,3] This unusual alga produces three groups of hydrocarbons, namely, C_{23}−C_{31} alkadienes and trienes, C_{30}−C_{37} triterpenoids (botryococcenes), and a C_{40} tetraterpenoid (lycopadiene), characteristic of three separate races: A, B, and L. Race B is capable of synthesizing all three hydrocarbon groups. Its pyrolysis at around 400 °C yielded, in addition to hydrocarbons, ketones and fatty acids.[3]

An enigmatic rubbery deposit called coorongite, first reported in 1852 from Alfred Flat near the coastal settlement of Salt Creek in the Coorong district of South Australia, is now known to be the dried and microbiologically partly oxidized remains of blooms of *B. braunii*.[4−6] A comparison of their respective elemental compositions (Table 1) shows that the conversion of *B. braunii* race A into coorongite involves major losses of oxygen and nitrogen. Logically, this would entail removal of carbohydrate and protein components from the alga, for which the infrared (IR) spectra of coorongite and the freeze-dried alga provide some evidence.[7] It may require the intervention of bacteria,[5,8,9] which could also explain the lack of correspondence between their respective free aliphatic hydrocarbon fractions. Obvious differences include the absence of a strong predominance of odd- over even-carbon-numbered homologues among the C_{23+} *n*-alkanes in coorongite[5,8,10] and regular C_{18}−C_{20} isoprenoid alkanes in the alga.[5]

The highly aliphatic nature of coorongite is evident from its analysis by IR spectroscopy[4,7] and pyrolysis−hydrogenation−gas chromatography (PHGC).[7,8] By comparison to the IR spectrum of *B. braunii*, that of coorongite exhibits a marked enhancement of the characteristic alkyl absorption bands [C−H at 2940 and 2850 cm^{-1}, CH_2 and CH_3 at 1460 cm^{-1}, and

Received: March 13, 2012
Revised: May 13, 2012
Published: May 16, 2012

   dx.doi.org/10.1021/ef300451s | *Energy Fuels* 2012, 26, 3874−3881

Table 1. Elemental Compositions of Coorongite and Freeze-Dried *B. braunii* (Race A)

sample	C (%, on a dry and ash-free basis)	H (%, on a dry and ash-free basis)	N (%, on a dry and ash-free basis)	S (%, on a dry and ash-free basis)	O[a] (%, on a dry and ash-free basis)	H/C (atomic)	O/C (atomic)	reference
B. braunii	49.4	8.1	8.4	0.5	35.6	1.95	0.54	6
coorongite	71.6	10.9	0.8	1.1	15.7	1.82	0.16	6
	70.0	10.6	0.8	0.5	18.1	1.80	0.19	6
	72.7	10.9	0.6	0.4	15.4	1.79	0.16	6 and 7[b]
	79.7	12.0	0.7	0.1	7.5	1.79	0.13	9

[a]By difference. [b]The sample was analyzed in the present study.

$(CH_2)_n$, where $n > 4$, at 720 cm^{-1}], a reduction of the broad band at 3370 cm^{-1} (O−H and N−H), and an augmentation of the 1050 cm^{-1} band by absorptions at 1090 and 1150 cm^{-1} (C−O). This is consistent with the aforementioned loss of algal carbohydrates and proteins and the development of ether linkages during oxidative polymerization of long-chain alkadienes.[11] The PHGC trace of coorongite pyrolyzed at 600 °C is dominated by C_6−C_{26} *n*-alkanes, with lesser amounts of C_7−C_{19} alkylbenzenes and the corresponding *n*-alkylcyclohexanes.[8] A subsequent study of coorongite using solid-state ^{13}C nuclear magnetic resonance (NMR)[12] allowed for the type of carbon to be quantified. It confirmed that the majority is in the form of $(CH_2)_n$, consistent with the presence of *n*-alkadienes (biomarkers of race A). However, small amounts of CH_3, possibly from botryococcenes (biomarkers for race B), were also detected.

Several problems may arise during biofuel production. One likely scenario is that algal biomass will be harvested and stockpiled to form dried residues, in which some microbiological activity and oxidation then occurs. We should note here that the potential of pyrolysis to process algae is debatable given their high water content and that their drying is energy-intensive, unless performed naturally in stockpiles. Because such material is analogous to coorongite, the latter is potentially a good model for exploring future issues in processing. Pyrolysis is a fast, simple method that can be used to evaluate potential oil yields[13] and, indeed, may be used on an industrial scale to produce oil from biomass. The present investigation employed a thermogravimetric analyzer (TGA) coupled to an IR instrument operating under non-isothermal conditions and a microreactor operating under isothermal conditions. Analysis of the pyrolysates yields important information about the hydrocarbons that can be volatilized. Here, we use gas chromatography−mass spectrometry (GC−MS), NMR, and IR spectroscopy.

The coorongite specimen analyzed in this study is from the original type locality.[4] It is fully characterized for its functional group content, and the structure of the pyrolysis products is also investigated. This material may be useful in future process design.

2. EXPERIMENTAL SECTION

2.1. Pyrolysis. *2.1.1. Isothermal Pyrolysis.* Isothermal pyrolysis was conducted using a three-port glass microreactor, in which pure nitrogen gas was directed across the surface of granulated coorongite (approximately 1 g, with a particle size < 1.6 mm) at a flow rate of approximately 190 mL/min and ambient pressure for 1.5 h. In this experiment, a sand bath was preheated to the operating temperature before immersing the microreactor to start the pyrolysis. To minimize temperature overshoot, the system was preheated to the desired temperature at a rate of 1 °C/min. Under such stringent conditions, the rapid heating rate of the sample to its isothermal temperature was achieved at approximately 10^4 °C/s.[14] The residence time, particle size, and gas pressure were kept constant, while the pyrolysis temperature was varied. With a continuous flow of nitrogen gas, each reaction is semi-batch. Pyrolysis was performed at temperatures of 359, 402, 452, 456, 480, and 520 °C. At temperatures of 359, 452, and 520 °C, the pyrolysate was collected by sorption using deuterated chloroform (1.4 mL) in a glass vial cooled to a sub-ambient temperature with ice to increase the condensable fraction.

2.1.2. Non-isothermal Pyrolysis. A simultaneous Netzsch STA 449 C Jupiter thermogravimetric analyzer coupled to a Bruker Vertex 70 infrared spectrometer (TGA−IR) was used to investigate the behavior of coorongite during non-isothermal pyrolysis. Granulated coorongite (approximately 20 mg) was weighed into an aluminum oxide crucible, covered with a pierced lid, and heated from ambient temperature to 1000 °C at a rate of 5°/min under high-purity N_2 at a flow rate of 50 mL/min for a period of 3.3 h.

2.2. Analysis. Table 2 lists NMR spectroscopic data for products and products. The products of coorongite pyrolysis are complex, and not all can be quantified by molecular techniques, such as GC−MS. Hence, in the present study, the bulk pyrolysate was also analyzed for structural group content by IR and NMR spectroscopy. However, caution is necessary when using these techniques quantitatively. In IR spectrometry, different structural moieties have different extinction coefficients. In solution ^1H NMR spectra, the overlap of functionality presents difficulties for quantitation. Solution ^{13}C NMR spectra can be better, provided that gated decoupling techniques are employed to reduce nuclear Overhauser and other effects that make peak heights not proportional to the concentration. Likewise, cross-polarization dynamics compromises the quantitative application of solid-state NMR. Nevertheless, together these techniques make a powerful characterization tool and are useful in setting quantitative limits on individual structural groups.

2.2.1. NMR Spectroscopy. Solid and solution NMR data were acquired using Bruker (200 MHz) and Varian (400 MHz) 9.4 T instruments, respectively, to examine the pyrolysate volatiles and residues. ^1H samples were spun at 20 Hz in a 5 mm NMR tube, employing a pulse width of 4.65 μs, an acquisition time of 3.703 s, a nil relaxation delay time, a 7.0 kHz sweep width, and 16 scans per sample. Approximately 0.1 mL of the collected volatiles was diluted to 0.6 mL with deuterated chloroform prior to the NMR analysis. The weight concentrations of the structural groups were derived from their corresponding proton peaks. For the sp^3C−H category, peaks belonging to the −CH< (1.4−1.7 ppm), $-CH_2$ (1.2−1.4 ppm), and $-CH_3$ (0.8−1.0 ppm) groups were integrated. The integrated peaks were divided by their corresponding proton numbers of 1, 2, and 3 and then multiplied by 13, 14, and 15, respectively, to give the stoichiometric weights of each structural group (see Table 2). Similarly, for the sp^2C−H category, proton peaks were assigned to $R_2C{=}CHR$ (5.2−5.7 ppm), $R_2C{=}CH_2$ (4.6−5.0 ppm), $R_2C{=}CHCH_3$ (1.6−1.9 ppm), and aromatic hydrogen (6.0−9.0 ppm), while carbonyl proton signals were assigned to ketones of mainly $-CH_2COCH_2-$ structure (2.1−2.6 ppm). The stoichiometric weights were calculated by multiplying by 24 ($R_2C{=}CHR$, $R_2C{=}CH_2$, $R_2C{=}CHCH_3$, and aromatic) and 28 ($-CH_2COCH_2-$). No OH group signals were detected. ^{13}C NMR cross-polarization magic angle spinning (CPMAS) spectra were obtained for coorongite and its pyrolytic residues at 50 MHz. Samples were spun at 5 kHz in a 4 mm

Table 2. ^{1}H NMR Data on the Volatiles in Three Isothermal Pyrolysates of Coorongite

structural group	pyrolysis temperature (°C)	fraction of the total integral as a proton signal (I)	stoichiometry factor (s)	corrected stoichiometry (I/s)	relative weight of the structural group (R) (g)	stoichiometric weight (RI/s) (g)
−CH<	359	0.24	1	0.24	13	3.12
−CH<	452	0.18	1	0.18	13	2.34
−CH<	520	0.17	1	0.17	13	2.21
$-CH_2-$	359	0.39	2	0.20	14	2.80
$-CH_2-$	452	0.50	2	0.25	14	3.50
$-CH_2-$	520	0.48	2	0.24	14	3.36
$-CH_3$	359	0.06	3	0.02	15	0.30
$-CH_3$	452	0.09	3	0.02	15	0.30
$-CH_3$	520	0.05	3	0.02	15	0.30
$R_2C{=}CHR$	359	0.06	1	0.06	24	1.44
$R_2C{=}CHR$	452	0.06	1	0.06	24	1.44
$R_2C{=}CHR$	520	0.09	1	0.09	24	2.16
$R_2C{=}CH_2$	359	0.02	2	0.01	24	0.24
$R_2C{=}CH_2$	452	0.02	2	0.01	24	0.24
$R_2C{=}CH_2$	520	0.05	2	0.03	24	0.72
$R_2C{=}CHCH_3$	359	0.07	3	0.04	24	0.96
$R_2C{=}CHCH_3$	452	0.05	3	0.02	24	0.48
$R_2C{=}CHCH_3$	520	0.06	3	0.02	24	0.48
ArH	359	0.02	1	0.02	24	0.48
ArH	452	0.01	1	0.01	24	0.24
ArH	520	0.02	1	0.02	24	0.48
$-CH_2COCH_2-$	359	0.14	4	0.04	28	1.12
$-CH_2COCH_2-$	452	0.10	4	0.03	28	0.84
CH_2COCH_2	520	0.10	4	0.03	28	0.84

diameter zirconium oxide rotor with a kel-F cap. A pulse width of 4.6 μs was used with a contact time of 0.75 ms, acquisition time of 0.01 s, a delay time of 2 s, and a 25 kHz sweep width, with 5000 scans collected. The ranges [in parts per million (ppm)] for the assigned structural groups are as follows: sp^3 carbon, 0−45; *O*-alkyl, 45−110; sp^2 carbon, 110−160; and carbonyl/carboxyl, 160−210.[15−17]

2.2.2. IR Spectroscopy. A Bruker Vertex 70 IR instrument was used with attenuated total reflectance (ATR) for the data acquisition. Resolution was set at 1.00 cm^{-1} and 16 scans per sample. Corrections for extended ATR, baseline, and normalizations were performed on the raw absorption data. The latter were quantified in a similar fashion to the ^{1}H NMR data after first being corrected for extinction coefficients. Absorption coefficients for C═O/COOH (1710 cm^{-1}), sp^3C−H (2920 cm^{-1}), and OH (3430 cm^{-1}) of kerogenic materials and an extinction coefficient for alkene/aromatic C═C (1450 cm^{-1}) were taken from the literature.[18,19] While model compounds might provide more exact coefficients, the cited literature discusses the sources of error in generalizing or using individual compound values. Those used herein give the best quantitation, as deduced by previous workers. The absorption coefficients are converted to extinction coefficients by multiplying by the IR wavelength and dividing by 4π in accordance with the well-known Bouguer's equation $\varepsilon = \alpha\lambda/4\pi$,[20] where λ is the wavelength of light at that absorption. Using the Beer−Lambert law, the observed absorption (A_{obs}) was divided by the extinction coefficient (ε) to give the relative yield of the structural group (mg per cm^{-2}: see Table 3). Coorongite and oil shale kerogens are closely related in that they are products of the diagenesis of algal biomass, and therefore, their extinction coefficients may be expected to be similar.[21−23] Although the converted structural group extinction coefficients of different types of kerogen vary,[18] the standard errors of measurement for sp^3C−H and C═O/COOH are 2.1 and 0.9%, respectively, which are even lower than the errors of IR measurements incurred in this study and, hence, appropriate. More importantly, the use of constant extinction coefficient data from a chemically related material for each structural grouping is expected to introduce the same degree of error to the IR measurements, hence giving more meaningful information on the thermal evolution of the coorongite.

Table 3. ATR−FTIR Data on the Volatiles in Three Isothermal Pyrolysates of Coorongite

structural group	pyrolysis temperature (°C)	relative infrared absorbance (A/A_0)	extinction coefficient (cm^2/mg)	relative yield of the structural group (mg cm^{-2})
sp^3C−H	359	1.6	0.0041	391.4
	452	2.0	0.0041	489.2
	520	2.0	0.0041	489.2
C═C	359	0.7	0.0249	28.1
	452	0.69	0.0249	27.7
	520	1.2	0.0249	48.2
C═O/COOH	359	2.0	0.0159	125.9
	452	1.79	0.0159	112.6
	520	1.9	0.0159	119.6

2.2.3. GC−MS. Molecular analysis of the collected chloroform-soluble pyrolysate was achieved using an Agilent 7890A/5975C GC−MS system. An Agilent HP-5MS (5% phenylmethylsiloxane) fused silica capillary column of 30 m length, 0.25 mm internal diameter, and 0.25 μm coating thickness was used for the separation with helium carrier gas at a constant pressure of 7.65 psi. The sample (1 μL) was injected in the split mode at a ratio of 50:1. The oven was programmed from 50 to 325 °C at 15 °C/min and then held at 325 °C for 1 min, for a total run time of 19.33 min. Full scan data were acquired over a range of 50−550 amu at 2.9 scans/s.

3. RESULTS AND DISCUSSION

3.1. Non-isothermal Pyrolysis. The loss of mass during the non-isothermal pyrolysis of coorongite, as monitored by TGA, is shown in Figure 1. Most of the mass (approximately 80%) is lost below 500 °C, above which the rate of loss is much slower. Significant loss occurs between 360 and 506 °C. The TGA−Fourier transform infrared (FTIR) spectra of outgas at these temperatures are illustrated in Figure 2. At 360 °C

dx.doi.org/10.1021/ef300451s | Energy Fuels 2012, 26, 3874−3881

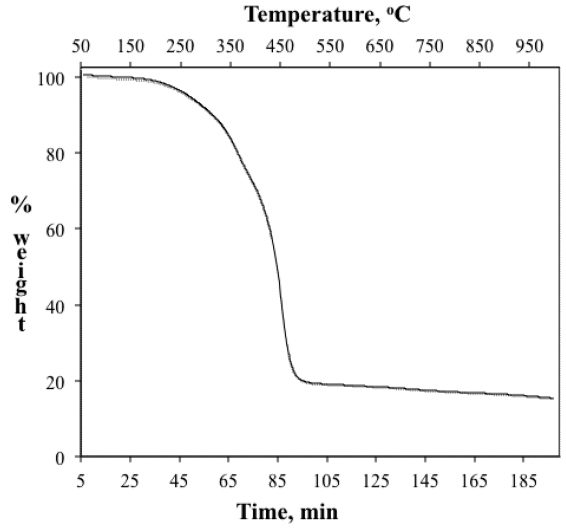

Figure 1. Plot of the percent weight against temperature and time during non-isothermal pyrolysis of coorongite.

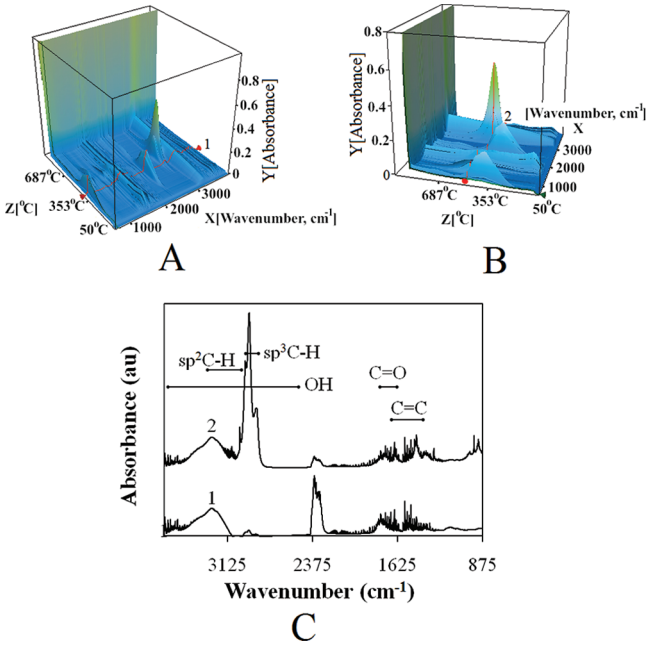

Figure 2. TGA–FTIR spectra of outgas from non-isothermal pyrolysis of coorongite. (A and B) Profiles of time of collection (z), absorption (y), and wavenumber (x), in which sampling times 1 and 2 correspond to gas evolution temperatures of approximately 360 and 506 °C, respectively. (C) Corresponding IR spectra.

(Figure 2A), the most intense peaks at around 2350 cm^{-1} may be assigned to carbon dioxide (spectrum 1 in Figure 2C). Also present are peaks for C═O/COOH, C═C, sp^2C–H, and OH, as well as some sp^3 carbon. It is well-known that decarboxylation occurs around 360 °C, in both brown coals and other natural materials. The same structural groups are present in the outgas at 506 °C (spectrum 2 in Figure 2C), except that the intensity of the sp^2 and sp^3 carbon peaks is significantly greater.

3.2. Isothermal Pyrolysis. At temperatures >350 °C, there is a strong linear relationship between the percent weight loss and temperature during the isothermal pyrolysis of coorongite

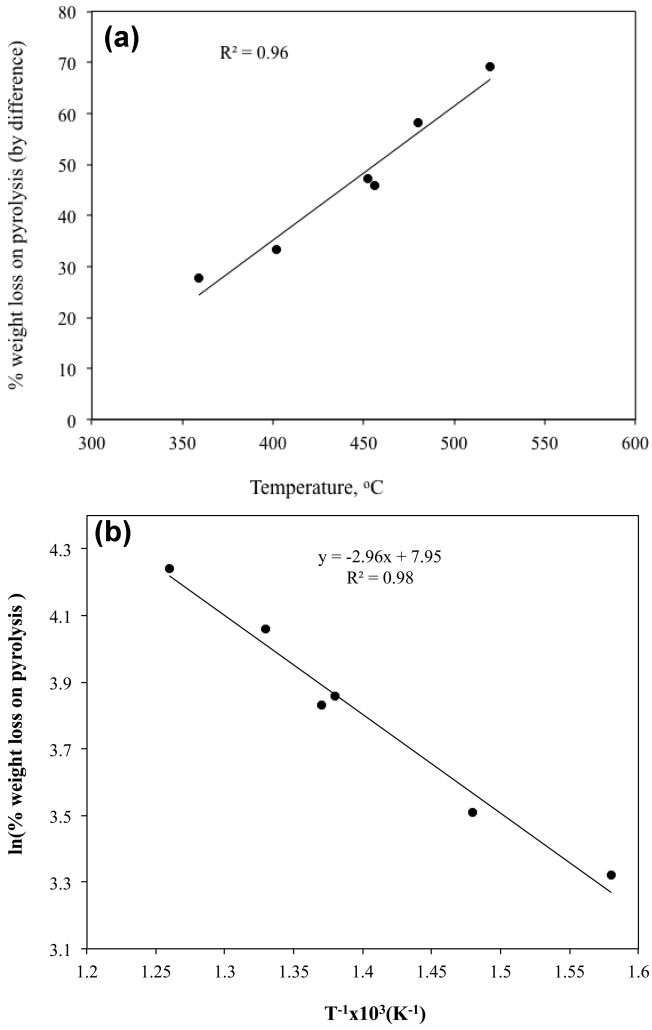

Figure 3. (a) Plot of the temperature versus percent weight loss upon isothermal pyrolysis of granulated coorongite for 1.5 h. (b) Arrhenius plot of the temperature versus percent weight loss upon isothermal pyrolysis of granulated coorongite for 1.5 h. The activation energy is calculated from the reciprocal slope (see the Appendix).

(Figure 3; slope = 0.26 wt %/°C). The corresponding plot of ln weight loss versus $1/T$ is also linear and gives an apparent activation energy of 25 kJ/mol. This value is much smaller than those for C–C bond cleavage in simple organic compounds and coal,[21] suggesting that volatilization of coorongite is in part a physical process. Indeed, it is closer to that observed for volatilization of oils. The reported activation energies for most oil shales, including those derived from *B. braunii*, are much higher (in the range 130–250 kJ/mol).[22−31] Of particular interest to the present investigation are two oil shales with lower activation energies. The Eocene Green River lamosite has an apparent activation energy of 62 kJ/mol,[32] while that of a Cretaceous Moroccan marinite is as low as 38 kJ/mol,[33] both calculated using methods similar to those employed here. The dominant maceral in each of these oil shales is lamalginite,[34,35] derived from planktonic algae. Significantly, in marinites, much of the precursor algal biomass has undergone partial bacterial degradation to bituminite and is volatile without pyrolysis. We do not attach too much attention to the exact values, but it is significant that coorongite is similar and indicates the ease by

dx.doi.org/10.1021/ef300451s | *Energy Fuels* 2012, 26, 3874–3881

which these types of deposits, including coorongite, are volatilized.

3.3. NMR and FTIR Characterization of Pyrolysate Volatiles. Quantitative ^{1}H NMR and ATR−FTIR data on the volatiles obtained by the pyrolysis of coorongite at three selected temperatures (viz. 359, 452, and 520 °C) are presented in Tables 2 and 3. The summed weight percentages of the structural groups sp^3C−H, C═C, and C═O for each method are then compared in Table 4.

Table 4. Comparison of ^{1}H NMR and ATR−FTIR Quantitation of the Volatiles in Three Isothermal Pyrolysates of Coorongite[a]

	^{1}H NMR (wt %)			IR (wt %)		
structural group	359 °C	452 °C	520 °C	359 °C	452 °C	520 °C
sp^3 C−H	69.3	77.0	69.3	71.8	77.7	74.5
C═C	16.3	12.9	20.3	5.2	4.4	7.3
C═O/COOH	14.4	10.1	10.5	23.1	17.9	18.2

[a]Standard errors of quantitation are as follows: NMR for sp^3C−H, 5.7%; C═O/COOH, 3.2%; C═C, 2.5% and IR for sp^3C−H, 5.6%; C═O/COOH, 4.5%; C═C, 1.0%. Phenols comprise part of the C═C signal.

Both spectroscopic methods concur in revealing that the composition of the volatiles does not change significantly with an increasing temperature of pyrolysis and that the bulk of the pyrolysable carbon (≥70%) is in the form of alkyl chains. Although IR spectrometry overestimates C═O/COOH at the expense of C═C, probably because of the use of inappropriate extinction coefficients, the trends in both analyses are in agreement.

3.4. Elemental and GC−MS Characterization of Pyrolysate Volatiles. Crude oil produced by the retorting of coorongite has the following elemental composition: 83.4% C, 11.6% H, 0.19% S, 0.56% N, and 4.25% O.[36] By comparison, other algal biofuels are much richer in the problematic heteroatoms oxygen and nitrogen, as illustrated by those derived from microalgal glycerides (39−63% C, 5−12% H, 4−12% N, and 22−53% O) and an algal pyrolysate (62% C, 9% H, 10% N, and 20% O).[37]

GC−MS analysis of the volatiles recovered from three isothermal pyrolysates of coorongite revealed the presence of a homologous series of C_9−C_{21} *n*-alkanes (*m*/*z* 57) and *n*-alkenes (*m*/*z* 55), C_8−C_{18} *n*-alkylbenzenes (*m*/*z* 91), and C_8−C_{12} *n*-ketones (*m*/*z* 58) (panels A and B of Figures 4 and 5, respectively). Also present but in lower abundance are *n*-alkanoic acids, phenols, and methylnaphthalenes (Table 5). The carboxylic acids produced at 359 and 452 °C are of relatively short carbon length (<C_{10}). Their thermal decarboxylation would skew the overall *n*-alkane distribution toward smaller carbon numbers.

Quantitation of the *m*/*z* 57 chromatograms (Figure 4A) demonstrates that the relative pyrolytic yields of heavier (C_{15+}) *n*-alkanes at 359 and 520 °C are identical ($\sum C_{15-21}/C_{15}$ = 3.2; Table 6). This in turn suggests that no chemical reactions were involved in their formation and that they were simply volatilized from the parent coorongite. However, this is not true for the shorter chain *n*-alkanes. Increasing the pyrolysis temperature from 359 to 452 °C shifts the maximum of the *n*-alkane distribution from C_{15} to C_9 (Figure 4A), reflecting the enrichment of the pyrolysate volatiles in alkanes with shorter carbon lengths. Accordingly, the ratio $\sum C_{9-14}/C_{14}$ at 452 °C is 4 times higher than at 359 °C (Table 6), confirming that the *n*-alkanes produced via thermal decarboxylation are <C_{15} in length.

The volatiles obtained from the pyrolysis of coorongite are heavily loaded with *n*-alkanes and *n*-alkenes. As such, they differ considerably from biofuels obtained from land or marine plants rich in glycerol esters.[1] Thus, *B. braunii* offers an alternative feedstock for biofuel production that does not involve the necessity to remove glycerol.

Molecular characterization of coorongite by the alternative methods of microscale-sealed-vessel (MSSV) thermal extraction at 300 °C for 2 h and pyrolysis at 325 °C for 24 h, both in tandem with GC−MS,[38,39] provides a somewhat different picture of its chemical structure, the details of which will be published elsewhere. Suffice to say that the off-line method employed in this study for the recovery of the pyrolysate volatiles (viz., dissolution in deuterated chloroform) does not capture the full molecular-weight range of the aforementioned compound classes. Nevertheless, it is sufficient for the comparisons made here.

3.5. ^{13}C NMR and ATR−FTIR Characterization of Coorongite and Its Solid Pyrolytic Residues. The data summarized in Table 7 show that, relative to the starting coorongite, its pyrolysis at 452 °C increased the amount of C═C carbon in the solid residue by 4−13% and its pyrolysis at 520 °C increased the amount of C═C carbon in the solid residue by 8−37%. In each case, the higher estimate was obtained by ^{13}C NMR spectrometry. The accompanying data indicate that this increase is due to the creation of C═C moieties and not the loss of other structural groups. The abundance of residual sp^3C−H is much higher at 452 °C (80−90%) than at 520 °C (62−85%). Therefore, it seems that, while some of the alkanes are volatilized at lower temperatures, others are lost from the

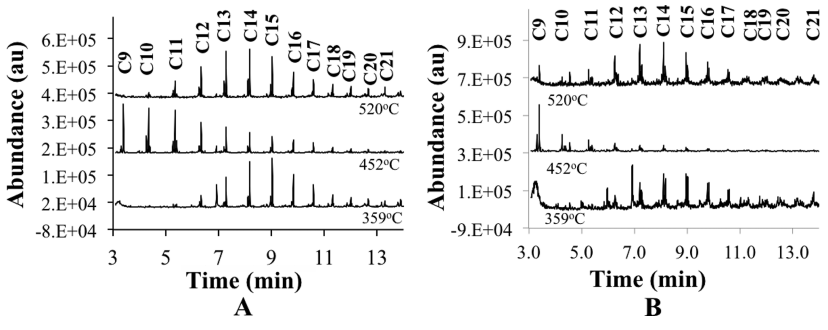

Figure 4. Mass chromatograms of aliphatic hydrocarbons from coorongite pyrolysis at 359, 452, and 520 °C. (A) *m*/*z* 57 (*n*-alkanes). (B) *m*/*z* 55 (*n*-alkenes).

dx.doi.org/10.1021/ef300451s | *Energy Fuels* 2012, 26, 3874−3881

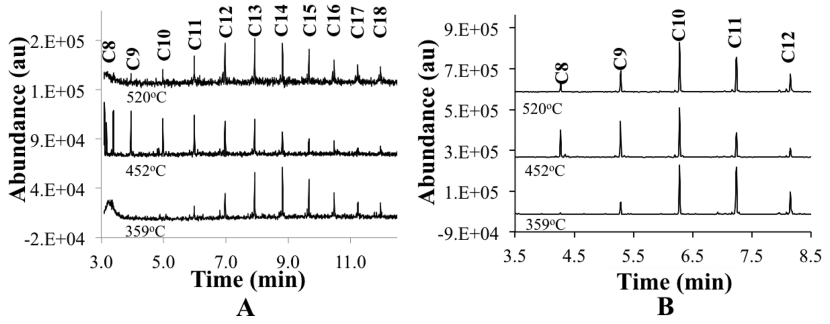

Figure 5. Mass chromatograms of aromatic hydrocarbons and ketones from coorongite pyrolysis at 359, 452, and 520 °C. (A) *m/z* 91 (*n*-alkylbenzenes). (B) *m/z* 58 (*n*-ketones).

Table 5. Carboxylic Acids, Phenols, and Naphthalenes Identified by GC−MS in the Volatiles from Three Isothermal Pyrolysates of Coorongite

pyrolysis products	359 °C	452 °C	520 °C
carboxylic acids	*n*-heptanoic acid	*n*-heptanoic acid	
	n-octanoic acid	*n*-octanoic acid	
	n-nonanoic acid	*n*-nonanoic acid	
	n-decanoic acid		
	phenol	phenol	phenol
phenols	2-methylphenol	2-methylphenol	2-methylphenol
	4-methylphenol	4-methylphenol	4-methylphenol
naphthalenes		2-methylnaphthalene	2-methylnaphthalene

Table 6. Relative Abundance of *n*-Alkanes (Normalized to C_{15}) in the Volatile Fractions from Three Isothermal Pyrolysates of Coorongite

	carbon number													summed yield		ratio	
temperature (°C)	9	10	11	12	13	14	15	16	17	18	19	20	21	$\sum C_{15-21}$ (S1)	$\sum C_{9-14}$ (S2)	$S1/C_{15}$	$S2/C_{14}$
359				0.2	0.4	0.6	1.0	0.7	0.7	0.2	0.2	0.2	0.2	3.2	1.2	3.2	2.0
452	3.8	1.7	1.4	1.3	1.0	1.3	1.0								10.5		8.1
520	0.5	0.1	0.3	0.6	0.9	0.8	1.0	0.7	0.7	0.2	0.2	0.2	0.2	3.2		3.2	

Table 7. Quantitation of Structural Groups in Coorongite and Solid Residues Resulting from Its Pyrolysis at 452 and 520 °C[a]

	fractional yield of the sample by weight			weight percent of the structural group			fractional yield of the structural group		
structural group	coorongite	452 °C	520 °C	coorongite	452 °C	520 °C	coorongite	452 °C	520 °C
sp^3 C−H	1.0	0.53	0.31	81.1	80.2	62.0	0.81	0.43	0.19
				87.5	89.9	85.4	0.88	0.48	0.26
C═C	1.0	0.53	0.31	1.3	14.4	38.0	0.01	0.08	0.12
				2.9	6.6	11.9	0.03	0.03	0.04
C−OH (as OH)	1.0	0.53	0.31	9.6	0.9	0	0.10	0	0
				1.6	0	0.4	0.02	0	0
C═O	1.0	0.53	0.31	8.0	4.5	0	0.08	0.02	0
				8.1	3.5	2.2	0.08	0.02	0.01

[a]Values are based on ^{13}C NMR (upper) and ATR−FTIR (lower) spectrometry.

residue at temperatures above 452 °C. This result is consistent with previous observations of the response of kerogens and coals to pyrolysis.[40] The TGA data presented in Figures 1 and 2 suggest that this second process occurs in the residue itself (rather than being a continuation of the earlier volatilization), but when formed, these new alkanes are immediately volatilized.

3.6. Implications for Biofuel Production. What is clear from the preceding discussion is that many of the volatiles released during the pyrolysis of coorongite are macromolecules. As such, they would need upgrading, for example, by catalytic cracking, hydrocracking, and hydrogenation, if similar *B. braunii* residues were to be used for biofuel production. Whether it would be worth pyrolyzing them before catalytic refining is debatable. The NMR and IR data in Table 4 indicate that sp^3C−H structures account for 69−75 wt % of the volatiles produced by pyrolysis at 520 °C, which in turn may well be easily cracked.

The corresponding data for the residue (Table 7) lacks internal consistency, possibly reflecting inappropriate extinction coefficients for condensed aromatic structures. Nevertheless, in suggesting that sp^3 carbon atoms comprise 62−85% of the residue, it does show that there is material that still could be

dx.doi.org/10.1021/ef300451s | *Energy Fuels* 2012, 26, 3874−3881

Table A1. Data for Arrhenius Calculations[a]

temperature (T) (K)	percent weight loss on pyrolysis by difference (k)	ln(k)	$10^3/T$
632	27.8	3.32	1.58
675	33.4	3.51	1.48
725	47.3	3.86	1.38
729	45.9	3.83	1.37
753	58.2	4.06	1.33
793	69.1	4.24	1.26

[a] $\ln k = -E_a/RT + \ln A$ obtained using simple methods[42] from DTA data.[43]

volatilized. Some of this residual carbon would be released by hydrocracking; therefore, it may be more worthwhile treating all of the material (i.e., volatiles plus residue) together.

The presence of C=C in biofuels is undesirable because of the possibility of sludge formation[41] and may mean that the oil produced from dried *B. braunii* residues, such as coorongite, would need to be hydrogenated before transportation. Furthermore, additional thermal treatment may be required to destroy the *n*-alkanoic acids, because acidic fuels have a tendency to corrode any metallic parts that they contact.

4. CONCLUSION

(1) Thermogravimetric analysis of naturally dried *B. braunii* blooms (coorongite) under nitrogen at near ambient pressure showed a total weight loss of 19% at 360 °C, increasing to 81% at 506 °C. Isothermal pyrolysis of coorongite in a microscale glass reactor under isothermal conditions at temperatures between 359 and 520 °C resulted in the generation of pyrolysate volatiles soluble in deuterated chloroform and also solid residues. The plot of the percent weight loss on pyrolysis against temperature demonstrates a linear relationship between these two variables. The apparent activation energy of 25 kJ/mol is very low and indicative of a physical process, possibly diffusion-controlled. (2) GC−MS analysis of the volatiles collected in deuterated chloroform from isothermal pyrolysis of coorongite at 359, 452, and 520 °C identified a homologous series of *n*-alkanes and *n*-alkenes (C_9−C_{21}), *n*-alkylbenzenes (C_8−C_{18}), and *n*-ketones (C_8−C_{12}), with lesser amounts of *n*-alkanoic acids, phenols, and methylnaphthalenes. The carboxylic acids are of relatively short carbon length, with their thermal decarboxylation explaining the shift of the *n*-alkane distribution toward lower carbon numbers at temperatures around 452 °C. The higher molecular weight *n*-alkanes (C_{15+}) are produced in a different way by simple volatilization. Alkenes and aromatic hydrocarbons are synthesized from the corresponding *n*-alkanes during pyrolysis. (3) Solid-state ^{13}C NMR and IR spectroscopy provided differing estimates of structural group abundance in the accompanying pyrolytic residues, possibly because of the use of inappropriate extinction coefficients for condensed aromatic moieties. Nevertheless, it appears that sp^3C−H structures comprise at least 62% by weight of the residues, suggesting that more of their carbon would be volatilized if treated by hydrocracking. (4) As a potential source of biofuel, stockpiled dried product from harvested *B. braunii* may benefit from the removal of carboxylic groups by pyrolysis. However, this will not negate the need for further upgrading by hydrocracking and hydrogenation.

APPENDIX

Data for Arrhenius calculations are provided in Table A1.

AUTHOR INFORMATION

Corresponding Author

*E-mail: k.kannangara@uws.edu.au.

Notes

The authors declare no competing financial interest.

ACKNOWLEDGMENTS

The coorongite examined in this study comes from the type locality (Alfred Flat) near Salt Creek, southeastern South Australia. The original specimen was part of the archival collection of the late Professor Sir Douglas Mawson, University of Adelaide. The authors are grateful to the CSIRO Energy Transformed Flagship for the Flagship Collaborative Projects Grant. Thanks are also due to Dr. Laurel George from the University of Western Sydney for the ^{13}C solid-state NMR analysis of the coorongite pyrolysate residues. The contributions of David McKirdy and Anthony Hall to this paper form TRaX Record #222.

REFERENCES

(1) Nag, A. *Biofuels Refining and Performance*; McGraw-Hill Prof Med/Tech: New York, 2007; p 312.
(2) Wake, L.; Hillen, L. *Mar. Freshwater Res.* **1981**, *32*, 353−367.
(3) Metzger, P.; Largeau, C. *Appl. Microbiol. Biotechnol.* **2005**, *66*, 486−496.
(4) Cane, R. F. *Geochim. Cosmochim. Acta* **1969**, *33*, 257−265.
(5) Douglas, A. G.; Eglinton, G.; Maxwell, J. R. *Geochim. Cosmochim. Acta* **1969**, *33*, 569−577.
(6) Dubreuil, C.; Derenne, S.; Largeau, C.; Berkaloff, C.; Rousseau, B. *Org. Geochem.* **1989**, *14*, 543−553.
(7) McKirdy, D. M. The diagenesis of microbial organic matter: A geochemical classification and its use in evaluating the hydrocarbon-generating potential of Proterozoic and Lower Palaeozoic sediments, Amadeus Basin, central Australia. Ph.D. Thesis, Australian National University, Canberra, Australia, 1977.
(8) McKirdy, D. M.; McHugh, D. J.; Tardif, J. W. *Biogeochemistry of Ancient and Modern Environments*; Australian Academy of Science: Canberra, Australia and Springer-Verlag: Berlin, Germany, 1980; pp 187−200.
(9) Glikson, M. *Org. Geochem.* **1983**, *4*, 161−172.
(10) Brooks, J. D.; Smith, J. W. *Geochim. Cosmochim. Acta* **1967**, *31*, 2389−2397.
(11) Cane, R. F.; Albion, P. R. *Geochim. Cosmochim. Acta* **1973**, *37*, 1543−1549.
(12) Wilson, M. A.; Batts, B. D.; Hatcher, P. G. *Energy Fuels* **1988**, *2*, 668−672.
(13) Williams, P. F. *Fuel* **1983**, *62*, 756−771.
(14) Solomon, P. R.; Colket, H. B. *Fuel* **1979**, *57*, 749−755.
(15) Knicker, H.; Almendros, G.; González-Vila, F. J.; Martin, F.; Lüdemann, H. D. *Soil Biol. Biochem.* **1996**, *28*, 1053−1060.
(16) Schmidt, M. W. I.; Knicker, H.; Hatcher, P. G.; Kogel-Knabner, I. *Eur. J. Soil Sci.* **1997**, *48*, 319−328.
(17) Petsch, S. T.; Smernik, R. J.; Eglinton, T. I.; Oades, J. M. *Geochim. Cosmochim. Acta* **2001**, *65*, 1867−1882.
(18) Verheyen, T. V.; Johns, R. B. *Geochim. Cosmochim. Acta* **1981**, *45*, 1899−1908.
(19) Datka, J.; Turek, A. M.; Jehng, J. M.; Wachs, I. E. *J. Catal.* **1992**, *135*, 186−199.
(20) Spitzer, W. G.; Fan, H. Y. *Phys. Rev.* **1957**, *106*, 882−890.
(21) Serio, M. A.; Hamblen, D. G.; Markham, J. R.; Solomon, P. R. *Energy Fuels* **1987**, *1*, 138−152.
(22) Yongjiang, X.; Huaqing, X.; Hongyan, W.; Zhiping, L.; Chaohe, F. *Oil Shale* **2011**, *28*, 415−424.
(23) Burnham, A. K.; Braun, R. L.; Samoun, A. M. *Org. Geochem.* **1988**, *13*, 839−845.

(24) Burnham, A. K.; Braun, R. L.; Gregg, H. R.; Samoun, A. M. *Energy Fuels* **1987**, *1*, 452−458.
(25) Braun, R. L.; Rothman, A. J. *Fuel* **1975**, *54*, 129−131.
(26) Ballice, L.; Yüksel, M.; Saglam, M.; Schulz, H.; Hanoglu, C. *Fuel* **1995**, *74*, 1618−1623.
(27) Braun, R. L.; Burnham, A. K.; Reynolds, J. G.; Clarkson, J. E. *Energy Fuels* **1991**, *5*, 192−204.
(28) Tegelaar, E. W.; Noble, R. A. *Org. Geochem.* **1994**, *22*, 543−574.
(29) Behar, F.; Kressmann, S.; Rudkiewicz, J. L.; Vandenbroucke, M. *Org. Geochem.* **1992**, *19*, 173−189.
(30) Dogan, O. M.; Uysal, B. Z. *Fuel* **1996**, *75*, 1424−1428.
(31) Dessort, D.; Connan, J.; Derenne, S.; Largeau, C. *Org. Geochem.* **1997**, *26*, 705−720.
(32) Rajeshwar, K. *Thermochim. Acta* **1981**, *45*, 253−263.
(33) Thakur, D. S.; Nuttall, H. E. *Ind. Eng. Chem. Res.* **1987**, *26*, 1351−1356.
(34) Hutton, A. *Int. J. Coal Geol.* **1987**, *8*, 203−231.
(35) Dyni, J. R. Petrographic classification of oil shales. *Scientific Investigations Report*; U.S. Geological Survey: Reston, VA, 2006; 2005-5294, p 42.
(36) Crisp, P. T.; Ellis, J.; Hutton, A. C.; Korth, J.; Martin, F. A.; Saxby, J. D. *Australian Oil Shales: A Compendium of Geological and Chemical Data*; University of Wollongong: Wollongong, Australia, 1987; p 31.
(37) Bryan, Y.; Marrone, P. Sub- and supercritical water for the production of fuel and green chemicals from algae. *Proceedings of the Algae Biomass Summit 2011*; Minneapolis, MN, 2011; http://algaeconnect.crowdvine.com/attachments/0002/3651/Yeh_Bryan.pdf.
(38) Hall, P. A.; Watson, A. F. R.; Garner, G. V.; Hall, K.; Smith, S.; Waterman, D.; Horsfield, B. *Sci. Total Environ.* **1999**, *235*, 269−276.
(39) Hall, A. P.; McKirdy, D. M.; Halverson, G. P.; Jago, J. B.; Gehling, J. G. *Org. Geochem.* **2011**, *42*, 1324−1330.
(40) Wilson, M. A. *NMR Techniques and Applications in Geochemistry and Soil Chemistry*; Pergamon: Oxford, U.K., 1987; p 353.
(41) Tran, N. H.; Bartlett, J. R.; Kannangara, G. S. K.; Milev, A. S.; Volk, H.; Wilson, M. A. *Fuel* **2010**, *89*, 265−272.
(42) Levine, R. D. *Molecular Reaction Dynamics*; Cambridge University Press: Cambridge, U.K., 2005.
(43) Milev, A. S.; Wilson, M. A.; Kannangara, G. S. K.; Feng, H.; Newman, P. A. *J. Phys. Chem. A* **2012**, *116*, 150−157.